MICHIGAN STATE UNIVERSITY

CYCLOTRON LABORATORY

MIGMA DISTRIBUTION FUNCTIONS AND FUSION RATES

M.M. GORDON and FELIX MARTI

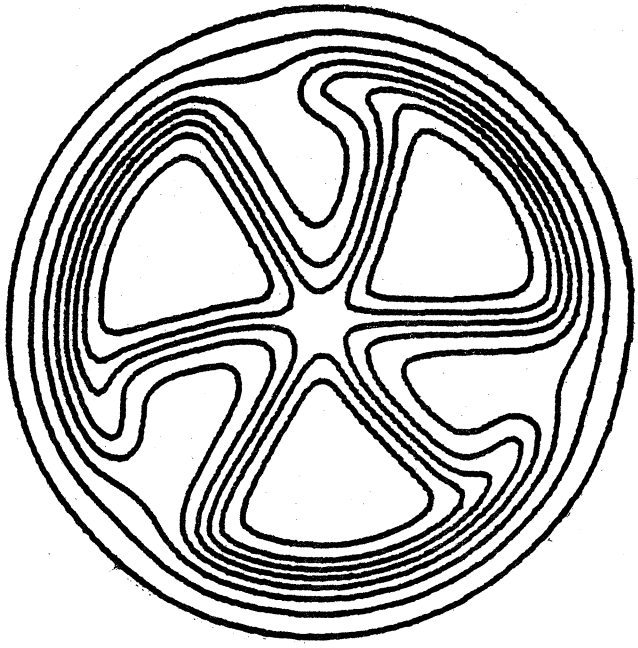

MSUCL-191 SEPTEMBER 1975

Migma Distribution Functions and Fusion Rates*

M. M. Gordon and Felix Marti
Cyclotron Laboratory and Physics Department
Michigan State University, East Lansing, Michigan, USA 48824

*Work supported by the National Science Foundation.

ABSTRACT

Using a circular orbit model appropriate to a Migma fusion device, analytical expressions are obtained for the particle density and the colliding pair distribution functions in terms of a parameter which specifies the central ("core") density. Contrary to expectations, our distribution functions tend to favor colliding pairs with low relative velocities, and this tendency grows stronger as the central density increases. The reaction rate parameters for the d+d and d+^{3}He fusion reactions have been calculated for a wide range of deuteron energies, and our resultant values are not only significantly smaller than those found by Maglich, but are also generally smaller than those obtained from a comparable Maxwell distribution. We also find that the total pair density and the resultant fusion rate increase remarkably little with large increases in the central density, so that this basic Migma characteristic does not appear particularly advantageous for fusion production. Finally, the fusion time constant and power output from a deuteron Migma are estimated, with rather disappointing results.

1. Introduction

In his discussion of fusion rates in the "Migma Cell", Maglich[1] has emphasized the importance of two basic Migma properties, namely, the very high density of the central core, and the prevalence of nearly head-on collisions within this core. We report here on a systematic analysis of these properties with results which are more detailed and less favorable than those presented by Maglich.

Our analysis is based on a circular orbit model which is a sophisticated version of the model used by Harrison[2], and much earlier by Haegi[3]. This model replaces the actual precessing orbits by circles, all of which pass within a small distance r_o of the magnetic field axis (r=0). Maglich, Harrison, and Haegi consider r_o to be determined by the size of the focused beam spot or by the energy spread of the injected ions. However, these considerations determine only the minimum value of r_o, while its steady state value (after elastic collisions are considered) may be much larger. We shall therefore treat r_o as a "compactness parameter", with values ranging up to r_o=0.1a, where a is the average radius of the circular orbits. As shown by Haegi[3], the central core density is inversely proportional to r_o.

As usual, our analysis assumes the ion distribution to be axially symmetric and time independent. We further assume that p_z/p for the ions can be neglected, and that the density does not depend on z within an unspecified range Δz. These assumptions simplify the problem sufficiently so that analytical results can be derived for the important Migma distribution functions. These functions then provide a clear and direct means for evaluating

those quantities which determine the fusion rates.

For a system of self-colliding particles having a spatial density $\rho(r)$, the reaction rate per unit volume at a specified position r is given by:

$$dI/dV = \tfrac{1}{2}\rho^2(r)\langle v_{12}\sigma(v_{12})\rangle_r, \qquad (1)$$

where v_{12} is the relative velocity of an ion pair, and $\sigma(v_{12})$ is the cross section. Here, the subscript r on the angular brackets indicates that the averaging is carried out at the specified position. That is, unlike the simple case of a plasma, the relative velocity distribution in a Migma depends on position.

Integration of the above formula yields the following result for the total reaction rate:

$$I = P\langle v_{12}\sigma(v_{12})\rangle, \qquad (2)$$

where $\langle v_{12}\sigma(v_{12})\rangle$ is the "reaction rate parameter", and where:

$$P = \tfrac{1}{2}\int\rho^2(r)dV, \qquad (3)$$

is the "total pair density". Our analysis is aimed at evaluating these quantities and showing how they depend on various parameters characterizing the Migma.

2. Migma Orbit Distribution

Since we apply the methods of dynamics to solve a problem which is inherently geometric, it proves convenient to set the frequency $\omega = qB_o/mc = 1$, and the mass m=1. In these units, the orbit period $\tau = 2\pi$, and the momentum p becomes identical to the

orbit radius. In addition, the (generalized) angular momentum K is then given by:

$$K = rp_\theta - \frac{1}{2} r^2, \tag{4}$$

which corresponds to motion in a uniform magnetic field, B_o.

Since the density is independent of z, we can ignore this coordinate with the understanding that $n=N/\Delta z$, where N is the total number of ions. Because of axial symmetry and time independence, the phase space distribution can be expressed as follows:

$$dn = (n/2\pi\tau)W(K,E)dtdEd\theta dK, \tag{5}$$

where W(K,E) is a normalized distribution function, that is

$$\int W(K,E)dKdE=1. \tag{5a}$$

In order to make this dn expression more relevant, we make use of the following identities:

$$dtdEd\theta dK=rdrd\theta dp_r dp_\theta, \tag{6a}$$

$$dp_r dp_\theta=pdpd\phi=dEd\phi, \tag{6b}$$

where the momentum angle ϕ is obtained from:

$$\cos\phi = p_\theta/p = (r^2+2K)/2rp, \tag{7}$$

as follows from (4). After dividing by $rdrd\theta$, eq. (5) then becomes:

$$dN/dV = (n/2\pi\tau)W(K,E)dEd\phi, \tag{8}$$

which provides a differential form of the density.

Although more general cases have been considered, we shall present detailed results here for only one special distribution function, since these results are the simplest analytically. In this case, the energy distribution of the Migma ions is assumed to be very narrow, so that the following replacements become possible:

$$p \to \langle p \rangle = a, \tag{9a}$$

$$W(K,E)dE \to W(K). \tag{9b}$$

This distribution is then equivalent to one in which all the orbits have the same radius, a. In this case, we then have:

$$dN/dV = (n/2\pi\tau)W(K)d\phi, \tag{10}$$

for the differential density.

As noted in the introduction, our model assumes that all orbits pass within a small distance r_o of the origin, and it then follows from (4) that K has the following limits:

$$K_{max,min} = \pm ar_o - \tfrac{1}{2}r_o^2, \tag{11}$$

where we have now set p=a. Since W(K) is normalized, and since its detailed form is unknown, we shall replace this function by its average value within the above limits, so that:

$$W(K) \to 1/2ar_o. \tag{12}$$

The differential density (10) now becomes:

$$dN/dV = (n/4\pi\tau ar_o)d\phi$$
$$= (a\rho_o/\pi r_o)d\phi, \tag{13}$$

where we have introduced the average density ρ_o given by:

$$\rho_o = n/4\pi a^2, \tag{14}$$

which corresponds to a uniform distribution of the ions throughout the Migma volume. We have also said $\tau=\pi$ in (13), since it proves more convenient to work with half periods by using the orbit symmetry; as a result, ϕ will lie between 0 and π.

3. Spatial Density

A circle of radius a and specified K value will extend from r_{min} to r_{max}, and these limits can be calculated from (4) by setting $p_\theta=\pm a$. Our model is concerned with a distribution of circles satisfying the condition, $r_{min}<r_o$, and in this case, we have:

$$2a-r_o<r_{max}<2a+r_o, \tag{15}$$

for the complete distribution. For a given r_o value, our Migma density will therefore vanish beyond $r=2a+r_o$.

The spatial density $\rho(r)$ is obtained by integration of (13), which yields:

$$\rho(r) = (a\rho_o/\pi r_o)[\phi_2(r)-\phi_1(r)], \tag{16}$$

where ϕ_1 and ϕ_2 are found from (11) and (7) to be:

$$\phi_{1,2} = \cos^{-1}[(r^2-r_o^2 \pm 2ar_o)/2ar], \tag{17a}$$

subject to the following restrictions:

$$\phi_1 = 0, \phi_2=\pi, \text{ for } r<r_o, \tag{17b}$$

$$\phi_1 = 0, \text{ for } r>2a-r_o. \tag{17c}$$

That is, for $r<r_o$, only the circles with $r_{min}<r$ can contribute, while for $r>2a-r_o$, only those with $r_{max}>r$ can be counted.

The above density function can be divided into three overlapping zones, which we discuss in turn in the following subsections. All our density calculations were based on the exact formulas above, and not on the approximations included below for purposes of clarification.

3.1 Central zone, $r<\sqrt{(2ar_o)}$. In this zone, which includes the "core", the quantity $r_o\rho(r)$ depends almost exclusively on r/r_o. This behavior is demonstrated in fig. 1 which applies to all $r_o\leq 0.1a$. For $r<r_o$ specifically, the density has its maximum value and is given by:

$$\rho(r<r_o) = \rho_{max} = a\rho_o/r_o. \tag{18}$$

In the remainder of this zone, the following formula provides a good approximation:

$$\rho(r_o<r<<a)\simeq(2a\rho_o/\pi r_o)\sin^{-1}(r_o/r). \tag{19}$$

The above formulas show that for very small r_o values, the density in this zone can reach very high values, which is a basic Migma property recognized by all previous authors. However, the total number of particles within this zone is nearly proportional to r_o, so that the net pair density here is practically independent of r_o.

3.2 Intermediate zone, $r_o<<r<<2a$. In this relatively broad zone, the density becomes nearly independent of r_o, and can be approximated by:

$$\rho(r_o<<r<<2a)\simeq(4a^2\rho_o/\pi r)(4a^2-r^2)^{-1/2}, \qquad (20)$$

which is the same as the formula given by Maglich[1] in his eq. (1).

The minimum density occurs at $r\simeq\sqrt{2}a$, and is given by:

$$\rho_{min} \simeq 2\rho_o/\pi, \qquad (21)$$

which is evidently independent of r_o. We should also note that the radius $r=\sqrt{2}a$ divides the Migma into two regions, an inner and outer region, each containing about half the particles as well as half the volume.

3.3 Outer region, $r>\sqrt{2}a$. In this region, the values of $\phi_1(r)$ and $\phi_2(r)$ appearing in the density formula (16) can be approximated by:

$$\phi_{2,1} \simeq [(2a\pm r_o-r)/a]^{1/2}, \qquad (22)$$

subject to the condition (17c) on ϕ_1 in the "periphery".

Before dropping to zero in the periphery, the density rises to a secondary maximum at $r=2a-r_o$, given approximately by:

$$\rho'_{max} \simeq (\rho_o/\pi)\sqrt{(2a/r_o)}. \qquad (23)$$

Since this peak varies as $1/\sqrt{r_o}$, it could be quite large for small r_o values. However, the number of particles inside this peak varies as $\sqrt{r_o}$, so that the net pair density here again is nearly independent of r_o.

4. Total Pair Density

The total pair density P, defined in (3), was calculated numerically using $\rho(r)$ obtained from (16,17) for seven values of r_o/a between 10^{-3} and 0.1. Fig. 2 shows a plot of the resultant

P values expressed in units of P_o, where:

$$P_o = \tfrac{1}{2}\rho_o n(\Delta z)=\tfrac{1}{2}N^2/4\pi a^2(\Delta z), \qquad (24)$$

which corresponds to a uniform distribution of N ions throughout the Migma volume.

The semi-log plot of fig. 2 also shows that the calculated points fall very close to the straight line given by:

$$P/P_o = 0.67+(3/\pi^2)\ell n(a/r_o). \qquad (25)$$

The constant term was determined empirically, and about 66% of this term comes from $r<2r_o$ in the central zone, while about 30% comes from $r>2a-r_o$ in the periphery. The log term was derived by analytical integration using the approximate density function (20) for $2r_o<r<2a-r_o$, and although we expected the result to be valid only for small r_o/a values, it is apparently still remarkably good even for $r_o/a=0.1$.

Although the details will be omitted here, we have also carried out calculations for the case of orbit distributions which, in addition to being characterized by the compactness parameter r_o, are also characterized by a radius (or momentum) spread, δa. The main effect of adding this parameter occurs in the outer region (sec. 3.3) where it lowers the density for $\delta a>r_o$. The following formula:

$$P/P_o=0.67+(1/\pi^2)\ell n[(a/r_o)^2(a/\delta a)], \qquad (26)$$

provides a good approximation to our numerical results when $\delta a>r_o$, and evidently reduces to (25) above when $\delta a=r_o$.

As noted in sec. 3.2, the radius $r=\sqrt{2}a$ divides the Migma into an inner and outer region each containing about half the

particles. Our P calculations also reveal that the inner and outer regions produce two-thirds and one-third of the total pair density, respectively.

The results given in fig. 2 and in the above formulas show that P/P_o changes rather slowly with r_o and δa. In particular, for a decrease in r_o/a by a factor of 10^2 (i.e., from 0.1 down to 10^{-3}), we find that P increases by only a factor of two when $\delta a = r_o$, and by a still smaller factor when $\delta a > r_o$. Over this same range in r_o/a, the central density increases from $10\rho_o$ up to $10^3\rho_o$, as shown by (18).

5. Intersecting Angle Distribution

The relative velocity v_{12} of a pair of particles can be expressed in terms of the angle α between their velocity vectors, as follows:

$$(v_{12})^2 = (v_1 - v_2)^2 + 4v_1 v_2 \sin^2(\alpha/2). \qquad (27)$$

If the velocity distribution of the ions has a relatively small width δv, then the first term will be of order $(\delta v)^2$, and may be neglected in the calculation of fusion rates. We assume this to be the case, and replace the second term by its average. This is practically equivalent to assuming that all ions have the same velocity v_o, and in this case, the above formula reduces to:

$$v_{12} = 2v_o |\sin(\alpha/2)|. \qquad (28)$$

We therefore need only find appropriate distribution functions for the angle α in order to evaluate the reaction rate parameters defined in eqs. (1,2).

For two ions moving in circular orbits, α corresponds to the angle of intersection between the two circles. Fig. 3 (a) illustrates this geometry for two identical circles passing close to the origin ($r_o \simeq 0$). In this case, the value of α is given by:

$$\alpha = 2 \cos^{-1}(r/2a), \qquad (29)$$

and therefore ranges from π at r=0 down to zero at r=2a. It should be noted that for any given r value, the circles have a second intersection with $\alpha \simeq 0$.

Fig. 3(b) shows a magnified picture of the central zone (sec. 3.1) for an orbit distribution characterized by the parameter r_o, and with a geometry corresponding to a fixed value of α. The picture clearly indicates that the resultant α distribution will be symmetric about $\alpha = \pi/2$, with peaks at both $\alpha = 0$ and π, for any r value within this zone. Moreover, the α distribution evidently becomes uniform for $r \to 0$.

To obtain analytical formulas for the α distributions, we start from the expression for dP, the number of pairs per unit volume in the volume element dV, given by:

$$dP = \tfrac{1}{2}\, dN dN'/dV, \qquad (30)$$

and then make use of the differential density (13) to obtain:

$$dP/dV = \tfrac{1}{2}(a\rho_o/\pi r_o)^2 d\phi d\phi'. \qquad (31)$$

Here, both ϕ and ϕ' range from ϕ_1 to ϕ_2 given in (17), so that the resultant distribution corresponds to a uniformly populated square in $\phi\phi'$-space.

Since ϕ and ϕ' lie between 0 and π, the momentum components are given by:

$$p_\theta = p\cos\phi,\ p_r = \pm p\sin\phi, \tag{32}$$

with the same for p'_θ and p'_r in terms of ϕ'. We then divide the pairs into (+) pairs and (-) pairs according as $p_r p'_r$ is positive or negative. Since α now is the angle between $\vec{p}$ and $\vec{p}'$, we then have:

$$\cos\alpha(\pm) = \cos\phi\cos\phi' \pm \sin\phi\sin\phi', \tag{33}$$

so that:

$$\alpha(+) = \phi - \phi',\ \alpha(-) = \phi + \phi', \tag{34}$$

for the two kinds of pairs. It proves advantageous to adopt these separate definitions of α, which then have the following limits for a given r value:

$$-\beta < \alpha(+) < +\beta,\ \gamma - \beta < \alpha(-) < \gamma + \beta, \tag{35a}$$

where β and γ are given by:

$$\beta(r) = \phi_2 - \phi_1,\ \gamma(r) = \phi_1 + \phi_2, \tag{35b}$$

with ϕ_1 and ϕ_2 obtained from (17). We should note here that $\beta(r)$ is proportional to $\rho(r)$, as can be seen from (16), and that $\gamma(r)$ reduces to (29) when $r_o \to 0$.

Returning now to the uniform square distribution (31) in $\phi\phi'$-space, we see that lines of constant $\alpha(+)$ or constant $\alpha(-)$ traverse this square parallel to one of the diagonals. Since there are equal numbers of (+) pairs and (-) pairs, the separate

dP/dV expressions for the two kinds of pairs are then given by:

$$dP_+/dV = \tfrac{1}{4}(a\rho_o/\pi r_o)^2(\beta - |\alpha(+)|)d\alpha(+), \tag{36a}$$

$$dP_-/dV = \tfrac{1}{4}(a\rho_o/\pi r_o)^2(\beta - |\gamma - \alpha(-)|)d\alpha(-), \tag{36b}$$

within the limits specified by (35), while both quantities are zero beyond these limits. These separate distributions therefore have exactly the same triangular shape (with base width 2β, and an altitude proportional to β), and differ only in that the first is centered at $\alpha(+)=0$, while the second is centered at $\alpha(-)=\gamma$.

The above pair distributions can be individually "folded" into the common α range, $0<\alpha<\pi$, and then added together to produce a combined pair distribution, dP/dV. We then use this result to define $W(r,\alpha)$, the normalized α distribution function, as follows:

$$dP/dV = \tfrac{1}{2}\rho^2(r)W(r,\alpha)d\alpha. \tag{37}$$

Having obtained $W(r,\alpha)$ in this way, we can then use (28) for v_{12} and calculate:

$$\langle v_{12}\sigma(v_{12})\rangle_r = \int v_{12}\sigma(v_{12})W(r,\alpha)d\alpha, \tag{38}$$

from the known cross section data. These results can then be used to evaluate the differential reaction rate given in (1). Although detailed descriptions will be omitted here, our distribution functions $W(r,\alpha)$ have all the properties expected from our prior discussion relating to fig. 3.

Given $W(r,\alpha)$, the intersecting angle distribution $W(\alpha)$ can then be obtained from:

$$PW(\alpha) = \frac{1}{2}\int \rho^2(r) W(r,\alpha) dV, \qquad (39)$$

where P is given in (3) and sec. 4. The total reaction rate parameter of eq. (2) can then be calculated from:

$$\langle v_{12}\sigma(v_{12})\rangle = \int v_{12}\sigma(v_{12}) W(\alpha) d\alpha, \qquad (40)$$

with the use again of (28) for v_{12}.

Fig. 4 shows plots of $W(\alpha)$ for different r_o/a values, as obtained from the calculations described above. These curves all have a primary peak at $\alpha=0$, with:

$$W(\alpha=0) = (a/\pi r_o)(P_o/P). \qquad (41)$$

After reaching a minimum near $\alpha=\pi/2$, $W(\alpha)$ then rises to a secondary peak which grows taller and closer to π as r_o/a decreases. However, this secondary peak always has a significantly smaller height and area than the primary one. As a result, we find that the median value of α decreases from 36° down to 12° as r_o/a declines from 0.1 down to 10^{-3}. Since half the pairs have α values less (or greater) than the median value, these results differ substantially from those of Maglich[1], who found that 80% of the pairs had $v_{12}>v_o$, which corresponds to $\alpha>60°$.

6. Reaction Rate Parameters

We consider first the case of a Migma containing only deuterons with (average) energy E_o. Data on the total fusion cross section for the two reactions, d+d→p+T and d+d→n+^{3}He, are presented in fig. 5, where the product $v\sigma$ is plotted against E_{lab}, the deuteron energy in the lab system.[4] This energy can be calculated for the Migma ions from:

$$E_{lab} = 4E_o \sin^2(\alpha/2), \qquad (42)$$

which assumes (28) to be valid. In this case, $0<E_{lab}<4E_o$.

Using $W(\alpha)$ functions like those shown in fig. 4, the reaction rate parameter of eq. (40) was calculated for values of E_o ranging from 0.1 MeV up to 2.0 MeV. Fig. 6 shows a plot of these results. Each plotted point represents an average for r_o/a values between 10^{-3} and 0.1. However, it is important to note that the results change surprisingly little over this broad r_o/a range, despite the large changes occurring in $W(\alpha)$ shown in fig. 4. The largest variation occurs at 2.0 MeV where $\langle v_{12}\sigma(v_{12})\rangle$ varies by ±6% from the value shown in fig. 6.

For comparison, fig. 6 also shows the total reaction rate parameter obtained from a Maxwell velocity distribution corresponding to the temperature T given by:

$$\langle E\rangle = E_o = (3/2)kT, \qquad (43)$$

which assumes the same average energy as in the Migma. As can be seen, these values of the reaction rate parameter range from 25% to 60% higher than the values obtained from our Migma distributions. Evidently, these Migma distributions are less effective per ion pair in the production of d+d fusion reactions.

We should also point out that our reaction rate parameters are smaller by a factor between 4 and 8 than those shown by Maglich[1] in his fig. 10 for the same E_o values. Specifically, in his eq. (21), Maglich quotes the value:

$$\langle v_{12}\sigma(v_{12})\rangle = 17 \times 10^{-16} \text{ cm}^3/\text{sec}, \qquad (44)$$

at E_o = 2.2 MeV, while our results yield the value: 2.1×10^{-16} cm^3/sec, for the same energy. However, the results given by Maglich exceed the maximum physical limit. That is, for E_o = 2.2 MeV, we have $E_{lab} < 8.8$ MeV, and from an extension of the data in fig. 5, it then follows that:

$$\langle v_{12}\sigma(v_{12})\rangle < 5.6 \times 10^{-16} \text{ cm}^3/\text{sec}, \qquad (45)$$

since the average cannot exceed the maximum value within the given interval.

7. Differential Reaction Rate

The differential reaction rate, dI/dr, which can be calculated from (1) and (38), provides detailed information concerning the relative distribution of fusion reactions in different regions of the Migma. As can be seen in fig. 5 for the d+d fusion reactions, the product $v\sigma$ increases monatonically with E_{lab} over the range considered here. This fact, together with (42), indicates that the Migma region characterized by large α values, namely the central zone, will predominate in producing fusion reactions. This is one of the Migma properties emphasized by Maglich[1], and it is confirmed by our results.

The central zone (sec. 3.1) extends from r=0 to $r=\sqrt{(2ar_o)}$, and therefore covers 2% to 21% of the full Migma radius $(2a+r_o)$ for r_o/a from 10^{-3} to 0.1, the values considered here. At E_o=2.0 MeV, our results show that this region accounts for about 60% of the fusion reactions, a result which varies by only ±3% over the large r_o/a range considered. By contrast, the outer region (sec. 3.3) where $r>\sqrt{2}a$, which contains half the particles, contributes only

11±3% in this case. At E_o = 0.1 MeV, the lowest energy we considered, the corresponding results are 64±5% for the central zone, and 4±2% for the outer region.

Within the central zone, our analysis shows that the product $r_o(dI/dr)$ depends almost exclusively on r/r_o. This property is demonstrated by the results given in fig. 7 for E_o = 2.0 MeV. As indicated by this plot, the maximum value of dI/dr invariably occurs at $r=r_o$. However, we should note that the fraction of the reactions occurring in $r<r_o$, for example, does depend on r_o. At E_o=2.0 MeV, this fraction changes from 16% to 28% as r_o/a increases from 10^{-3} to 0.1.

In his design of the Migma cell, Maglich chooses deuterons with E_o=2.2 MeV specifically in order that all fusion products escape except the ^{3}He ions. In this way, the deuterons "breed" a d+^{3}He Migma, which then yields a greater energy output. One problem with this scheme arises from the fact that the ^{3}He ions have a relatively broad distribution, one characterized by a much larger r_o value than that for the deuterons. That is, only a small percentage of the d+d reactions occur within $r<r_o$, as noted above.

8. d+^{3}He Migma

Our analysis can also be applied to the case of a d+^{3}He Migma provided we assume that the two kinds of ions are separately injected under carefully controlled conditions, so that they have the same orbit radius (a) and the same compactness parameter (r_o).

We then need only make the change:

$$\frac{1}{2} N^2 \rightarrow N_d N_h, \qquad (46)$$

in eq. (24) for P_o, with corresponding simple changes in other formulas involving P or I. Matching the orbit radius requires $v_h = 2v_d/3$ for $^3He^+$ ions, or $v_h = 4v_d/3$ for $^3He^{++}$ ions. Since the latter requires four times the energy input of the former, most of our calculations have been based on the $^3He^+$ case.

In order to provide a direct comparison with the d+d case, cross section data for the d+^{3}He fusion reaction are also presented in fig. 5, where the product $v\sigma$ is plotted against E_{lab}, the deuteron energy in the lab system. Because of the sharp resonance in the d+^{3}He reaction, the value of $v\sigma$ reaches a high peak at $E_{lab} = 0.44$ MeV and then decreases substantially. As we shall show, this decrease in $v\sigma$ produces a dramatic change in the reaction distribution within the Migma at higher energies.

If E_o is the deuteron energy in the Migma, then the corresponding value of E_{lab} can be calculated from:

$$E_{lab} = (E_o/9)(1+24 \sin^2\alpha/2), \qquad (47)$$

as follows from (27) with $v_1 = v_d$ and $v_2 = v_h = 2v_d/3$. With $E_o = 2.0$ MeV, for example, we find that $0<\alpha<\pi/4$ corresponds to $0.22 \text{ MeV} < E_{lab} < 1.0$ MeV, which brackets the peak in $v\sigma$ shown in fig. 5.

Using the same procedure as in sec. 6, the d+^{3}He reaction rate parameters were calculated for a wide range of E_o values, and the results are plotted in fig. 8. Here again, the plotted curve represents an average for r_o/a values between 10^{-3} and 0.1. As can be seen, the reaction rate parameter rises rapidly to a peak at $E_o = 0.2$ MeV, then declines to a minimum near 0.7 MeV, and finally

rises again out to E_o=3.0 MeV, at least. Here again, our reaction rate parameters are significantly smaller than those presented by Maglich[1] in his fig. 10 for the d+^{3}He case.

Fig. 8 also shows the reaction rate parameters calculated from a Maxwell distribution characterized by a temperature which we assumed was again given by eq. (43) in terms of E_o. As in the d+d case shown in fig. 6, these $\langle v_{12}\sigma(v_{12})\rangle$ values are uniformly higher than our Migma values below $E_o = 1.9$ MeV, where the two curves cross over.

The rise in the reaction rate parameter for the d+^{3}He Migma at energies above $E_o \simeq 1.0$ MeV can be understood in terms of the sharp peak in $W(\alpha)$ at $\alpha = 0$ in combination with the peak in $v\sigma$ at $E_{lab} = 0.44$ MeV discussed above. To show this, we consider the differential reaction rate given by:

$$dI/d\alpha = Pv_{12}\sigma(v_{12})W(\alpha), \qquad (48)$$

which reveals the contribution from different α regions to the reaction rate. Using $W(\alpha)$ shown in fig. 4 for $r_o/a = 0.01$, the values of $dI/d\alpha$ were calculated for E_o=0.1 MeV and 2.0 MeV. Fig. 9 shows the resultant curves, which have been normalized to provide a fair comparison. Evidently, at the higher energies, those collisions with small α values predominate in the production of d+^{3}He fusion reactions.

This phenomenon also manifests itself in the radial distribution of the fusion reactions. Using the procedure described in sec. 7, again with r_o/a values between 10^{-3} and 0.1, we obtain the following reaction percentages for the d+^{3}He case: (1) in the central zone, 66±6% at E_o=0.1 MeV, and 43±2% at E_o=2.0 MeV; (2) in the outer region, 0.9±0.4% at E_o=0.1 MeV, and 37±1% at E_o=2.0 MeV. These

results at E_o=0.1 MeV are very similar to those given in sec. 7 for the d+d case, since only the rapidly rising portion of the $v\sigma$ curve is involved here. The contrasting results obtained at E_o=2.0 MeV demonstrate that in cases like this, the fusion reactions are not concentrated in the central zone (or "core"), but are rather widely distributed throughout the Migma.

9. Conclusions

In accordance with eq. (2), the fusion rate is a product of the total pair density P and the reaction rate parameter $\langle v_{12}\sigma(v_{12})\rangle$. Our results for this parameter are shown in fig. 6 and fig. 8, respectively, for the d+d and d+^{3}He fusion reactions. As noted before, these results do not vary significantly with relatively large changes in the compactness parameter, r_o/a. Consequently, the compactness parameter influences the fusion rate mainly through the pair density P, which can be calculated quite accurately from eqs. (25,26), as shown in fig. 2.

According to Maglich[1], the primary feature of a Migma fusion device is its high density central core, which results from a highly ordered orbit distribution. We have considered such distributions with values of r_o/a ranging downward from 0.1 to 10^{-3}, which corresponds to a central density ranging upward from $10\rho_o$ to $10^3\rho_o$, where ρ_o is the average density. Over this broad range, the fusion rate increases by only a factor of two. We must therefore conclude that the high density central core does not provide a really significant advantage for fusion production.

Our results have been kept sufficiently general to apply to a variety of possible Migma configurations. Specific numerical values for the fusion rate can be obtained only by making additional assumptions regarding the density limit for a Migma. For this purpose, Maglich considered the limit imposed by space charge repulsion, and we shall adopt the same procedure in order to clarify certain differences.

If we assume for simplicity that the deuterons have a constant density ρ_o, then the vertical stability condition for motion close to the median plane becomes:

$$4\pi e^2\rho_o < m(\omega\nu_z)^2, \tag{49}$$

where ν_z is the magnetic focusing frequency (in oscillations per revolution) discussed in a previous paper[5]. To compensate for the inaccuracy of this relation, we make the following allowances: $\nu_z<1$, and $\omega<eB_o/mc$, where B_o is the peak field. The above space charge limit for the average density then reduces to:

$$\rho_o < B_o^2/4\pi mc^2. \tag{50}$$

Taking B_o=40 kG, a large but reasonable value, we then find:

$$\rho_o < 4\times10^{10} \text{ ions/cm}^3, \tag{51}$$

which is quite consistent with the limits obtained by Maglich, considering his use of B_o=200 kG.

The time constant τ_{dd} for the fusion reactions in a deuteron Migma is defined by:

$$-dN/dt = N/\tau_{dd} = 2I, \tag{52}$$

since two deuterons are consumed in each fusion. From eqs. (2,24), we then have:

$$1/\tau_{dd} = \rho_o(P/P_o)\langle v_{12}\sigma(v_{12})\rangle. \qquad (53)$$

If we now take E_o=2.2 MeV, the deuteron energy used by Maglich, and also take $r_o/a=10^{-3}$ in order to match his core density, then our results in fig. 2 and fig. 6, together with the ρ_o limit given above, lead to the following conclusion:

$$\tau_{dd}>5\times10^{4} \text{ sec}, \qquad (54)$$

which is a factor of 10^3 greater than the value given by Maglich in his eq. (45). Moreover, assuming his relaxation times for the multiple scattering losses are correct, then our much larger τ_{dd} value implies that a large fraction of the deuterons would be lost through multiple scattering processes. Ignoring these losses, and taking Δz=1.0 cm, we also find that the maximum power output is about 0.2 mW, which is 50 times smaller than the lower limit given by Maglich.

References

1. B. C. Maglich, Nucl. Instr. and Meth. 111(1973)213.
2. W. C. Harrison, Rutgers Migma Lab Report MIG-104-71(1971).
3. M. Haegi, Nouvelle Méthode de Confinément dans les Plasmas, Archives des Sciences, Université de Genève, 13, fasc.4(1960).
4. Cross section data were obtained from the following sources: N. Jarmie and J. D. Seagrave, Los Alamos Report LA-2014(1956); A. S. Ganeev, et al., Suppl. No. 5, Soviet Journal of Atomic Energy, (1958)21; J. L. Tuck, Nuclear Fusion 1(1961)201; R. L. Schulte, et al., Nuclear Physics A192(1972)609; T. W. Bonner, J. P. Conner, and A. B. Lillie, Phys. Rev. 88(1952) 473; W. E. Kunz, Phys. Rev. 97(1955)456; W. Grüebler, et al., Nuclear Physics A176(1971)631.
5. M. M. Gordon and D. A. Johnson, Nucl. Instr. and Meth., 121 (1974)461.

Figure Captions

Fig. 1. Density variation in the central zone. The plotted curve of $r_o\rho(r)$ versus r/r_o is nearly independent of r_o in the range shown for all $r_o<0.1a$. The vertical scale is determined by the maximum density, $\rho(r<r_o)=a\rho_o/r_o$, where ρ_o is the average density of the Migma. This curve also implies that the number of ions in this radial range is proportional to r_o.

Fig. 2. Total pair density P versus compactness parameter r_o/a. As can be seen, the straight line given by eq. (25) provides a good fit to the plotted points which were obtained from numerical integrations. The unit P_o is the total pair density corresponding to a uniform distribution of the ions throughout the Migma volume.

Fig. 3. Illustrations for the intersecting angle α. (a) At top, two identical circular orbits pass close to the origin 0, and intersect with an angle α between the velocity vectors at a given radius r. At any such radius, the circles have a second intersection with $\alpha\simeq 0$. (b) At bottom, a magnified picture of the central zone where the orbits can be approximated by straight lines. These orbits all pass within a small distance r_o of the origin, as indicated by the broken circle. The particular orbits shown here correspond to a fixed value of α.

Fig. 4. The normalized intersecting angle distributions $W(\alpha)$ for three different values of r_o/a: (a) 0.1, (b) 10^{-2}, (c) 10^{-3}. The primary peak at $\alpha=0$ is shown completely for curve (a) only. The other two curves reach the following primary peak values:

(b) 15.4, (c) 115. The dominance of the $\alpha=0$ peak is revealed by the median values of α: (a) 36°, (b) 21°, (c) 12°, which are indicated by the broken vertical arrows. The horizontal broken line at $W=1/\pi$ indicates the average value.

Fig. 5. Total cross section data for the d+d and d+^{3}He fusion reactions[4]. The product $v\sigma$ is plotted versus E_{lab}, the deuteron energy in the lab system, where v is the corresponding velocity. Although a much wider range of data was actually used in our calculations, the range shown here was purposely restricted so as to provide a direct comparison with the results shown in fig. 6 and fig. 8.

Fig. 6. The reaction rate parameter $\langle v\sigma\rangle$ for the d+d fusion reaction as a function of E_o, the deuteron energy in the Migma. The solid curve was calculated using our Migma distribution functions shown in fig. 4, with results which are insensitive to the r_o/a value. For comparison, the broken curve shows the results obtained from a Maxwell distribution having an average energy given by E_o. The scales here are exactly the same as those in fig. 5.

Fig. 7. Variation of the differential reaction rate within the central zone. The curve showing $r_o(dI/dr)$ versus r/r_o for $r<5r_o$ turns out to be nearly independent of r_o for all $r_o<0.1a$. This curve has been normalized to unity at $r=r_o$ and, as a result, it is at least qualitatively the same at all energies E_o. This curve also indicates that the number of reactions occurring within the range shown ($r<5r_o$) is independent of r_o.

Fig. 8. The reaction rate parameter for the d+^{3}He fusion reaction as a function of E_o, the deuteron energy in the Migma. The solid curve represents the results obtained using our Migma distribution functions shown in fig. 4. For comparison, the broken curve shows the results obtained from a Maxwell distribution having an average energy given by E_o. The scales here are exactly the same as in fig. 5.

Fig. 9. The differential reaction rate $dI/d\alpha$ for the d+^{3}He Migma at E_o=0.1 MeV and 2.0 MeV. These curves were obtained using the $W(\alpha)$ function shown in fig. 4 for $r_o/a=10^{-2}$. The curves are normalized to provide a fair comparison, and the horizontal broken line indicates the average value in both cases. The contrasting result at E_o=2.0 MeV serves to explain the increase in the reaction rate parameter shown in fig. 8 for E_o>1.0 MeV.

fig. 1

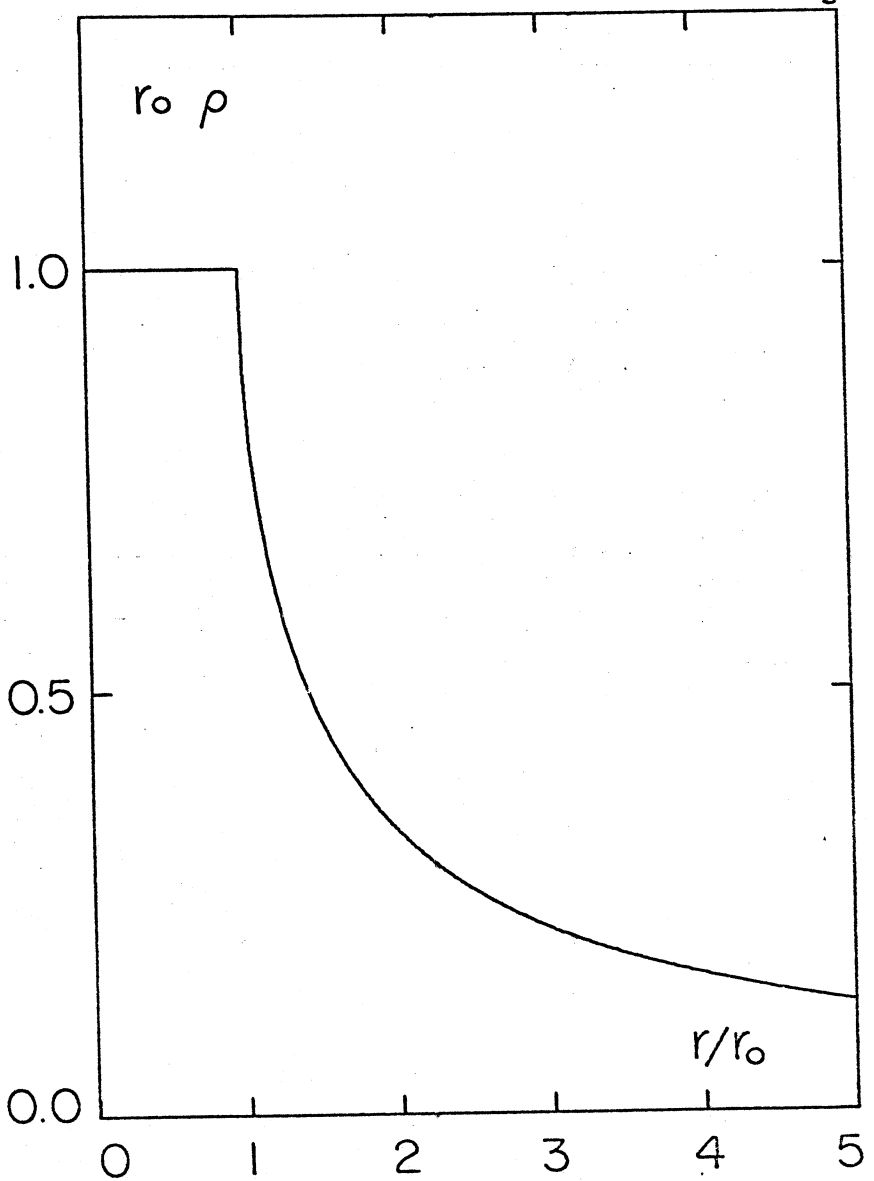

fig. 2

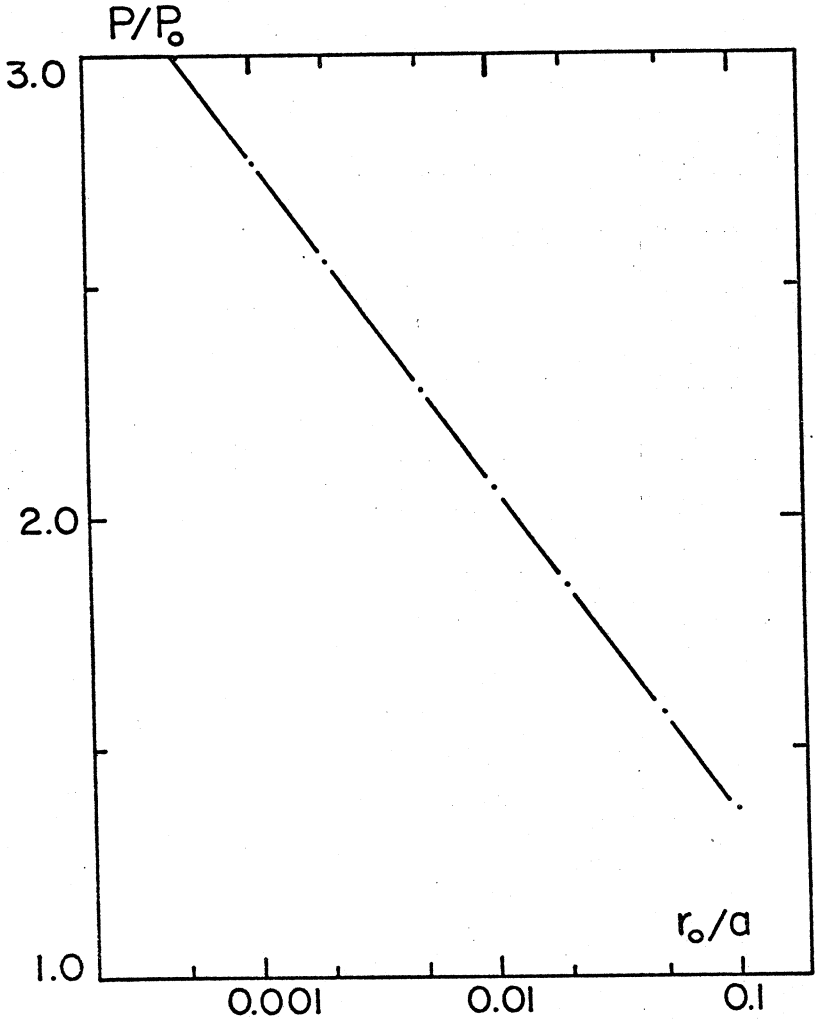

fig. 3

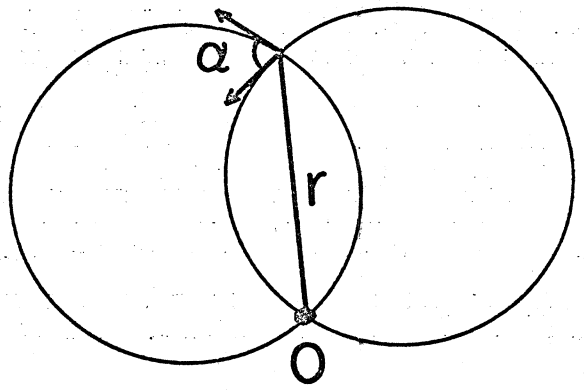

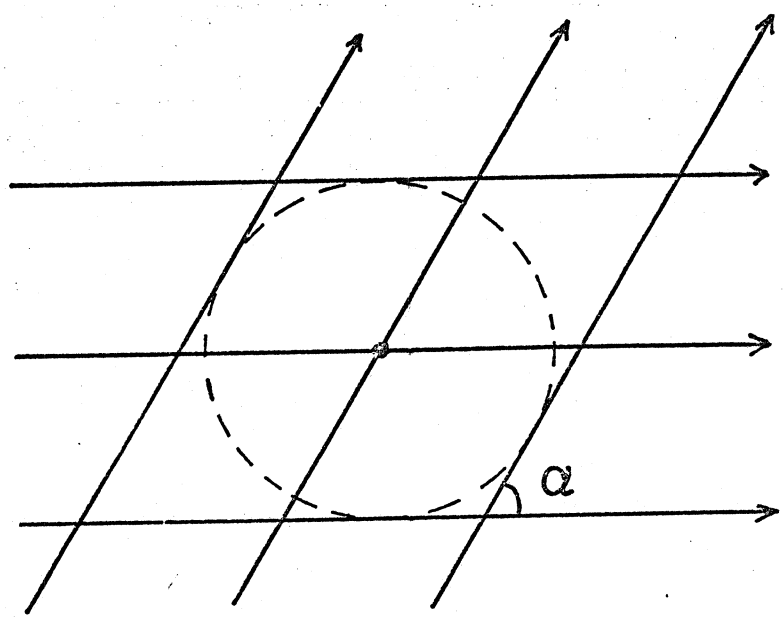

fig. 5

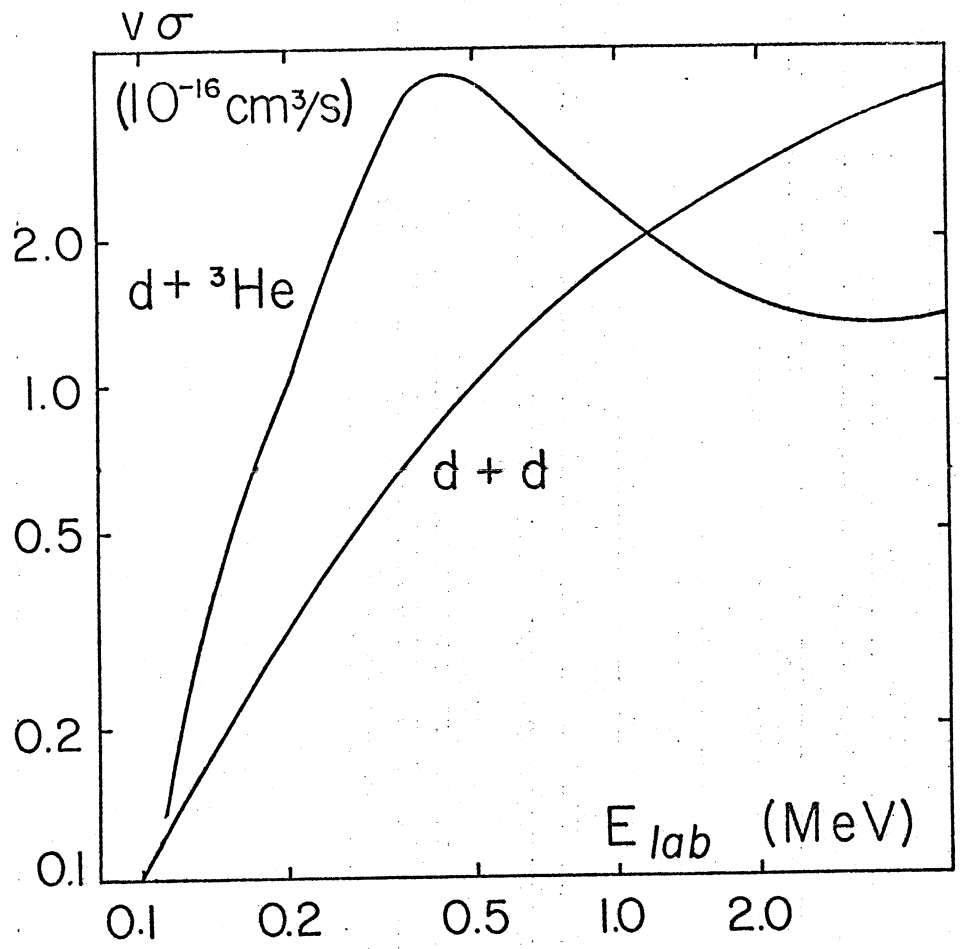

32

fig. 4

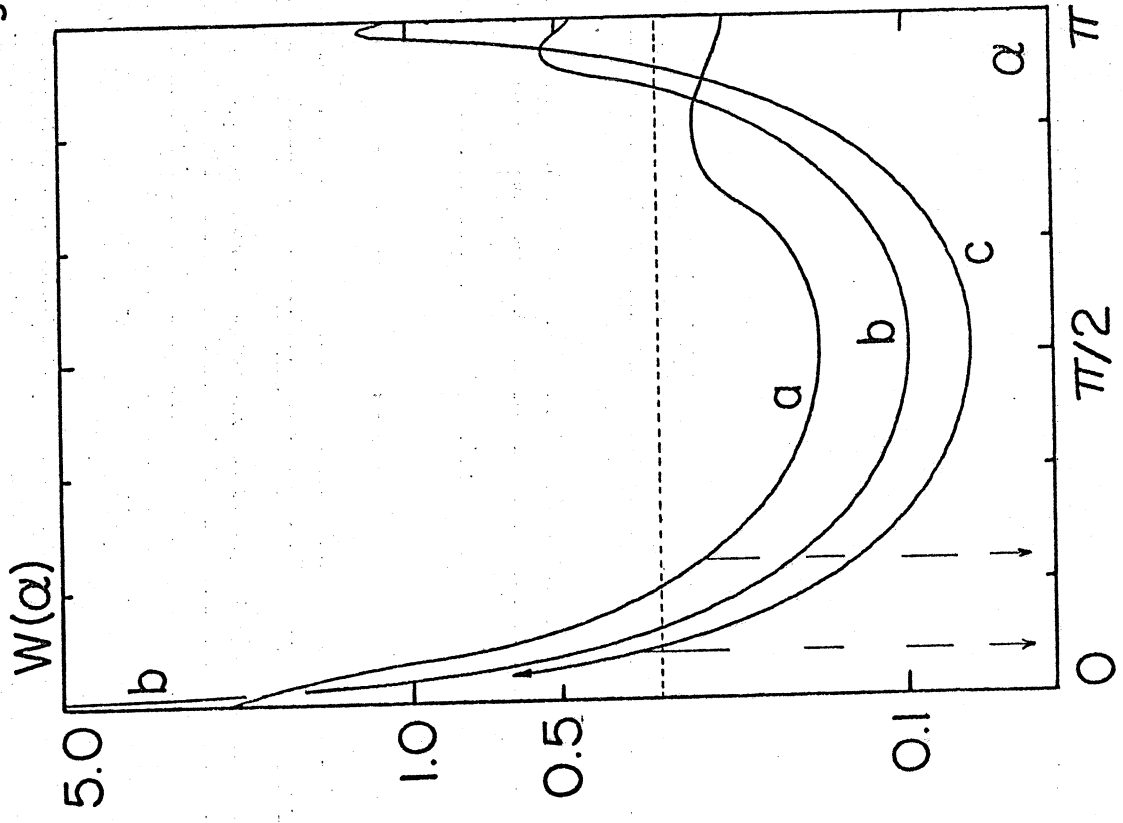

31

fig. 7

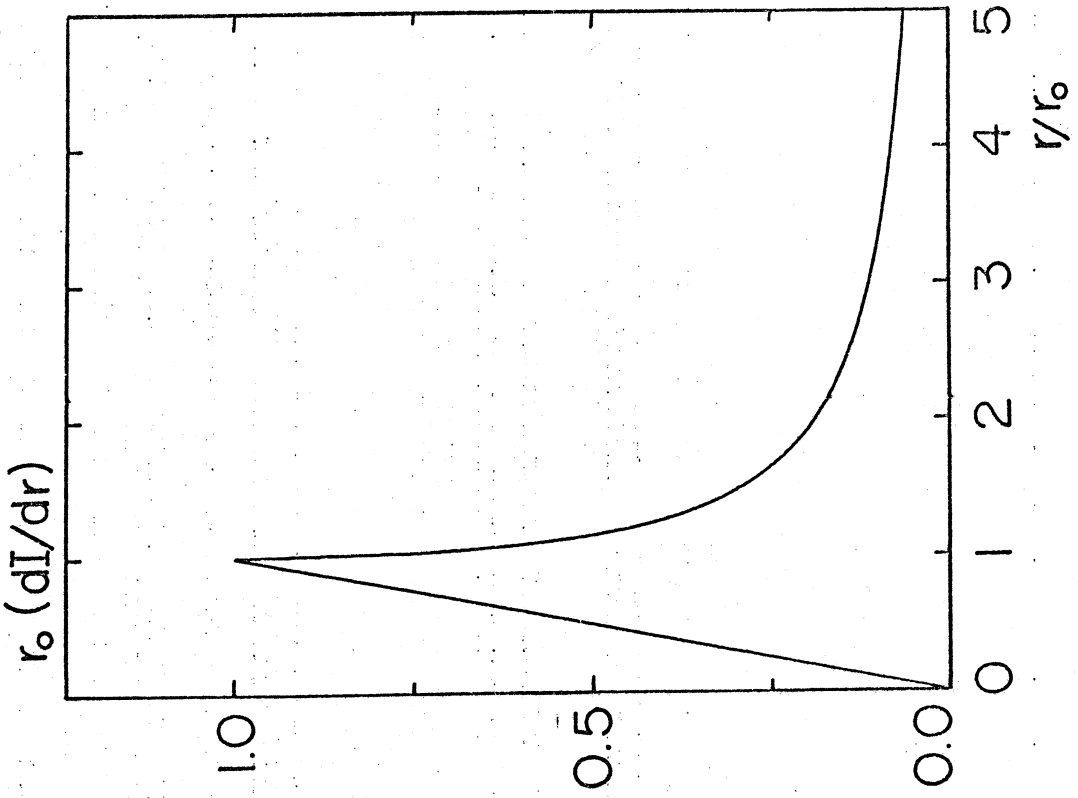
r/r₀
0
1
2
3
4
5
r₀ (dI/dr)
1.0
0.5
0.0

fig. 6

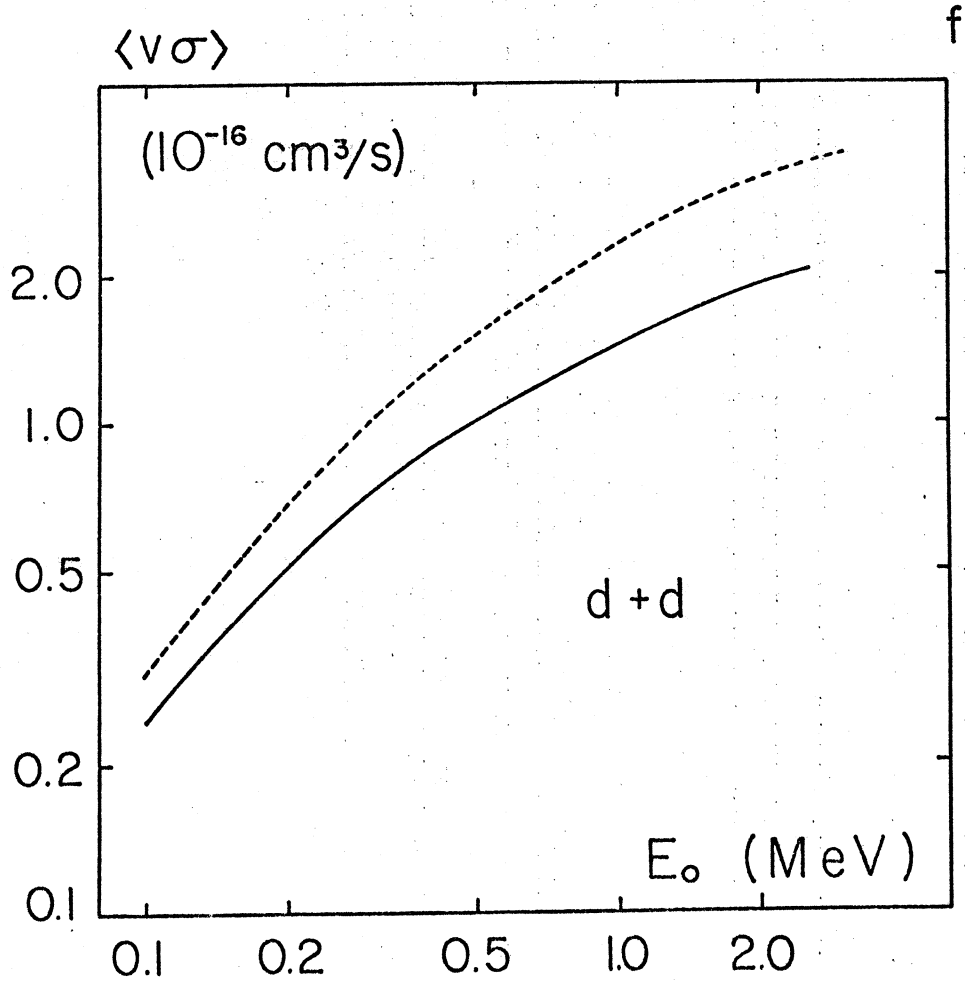
⟨vσ⟩
(10⁻¹⁶ cm³/s)
2.0
1.0
0.5
0.2
0.1
d + d
E₀ (MeV)
0.1
0.2
0.5
1.0
2.0

fig. 9

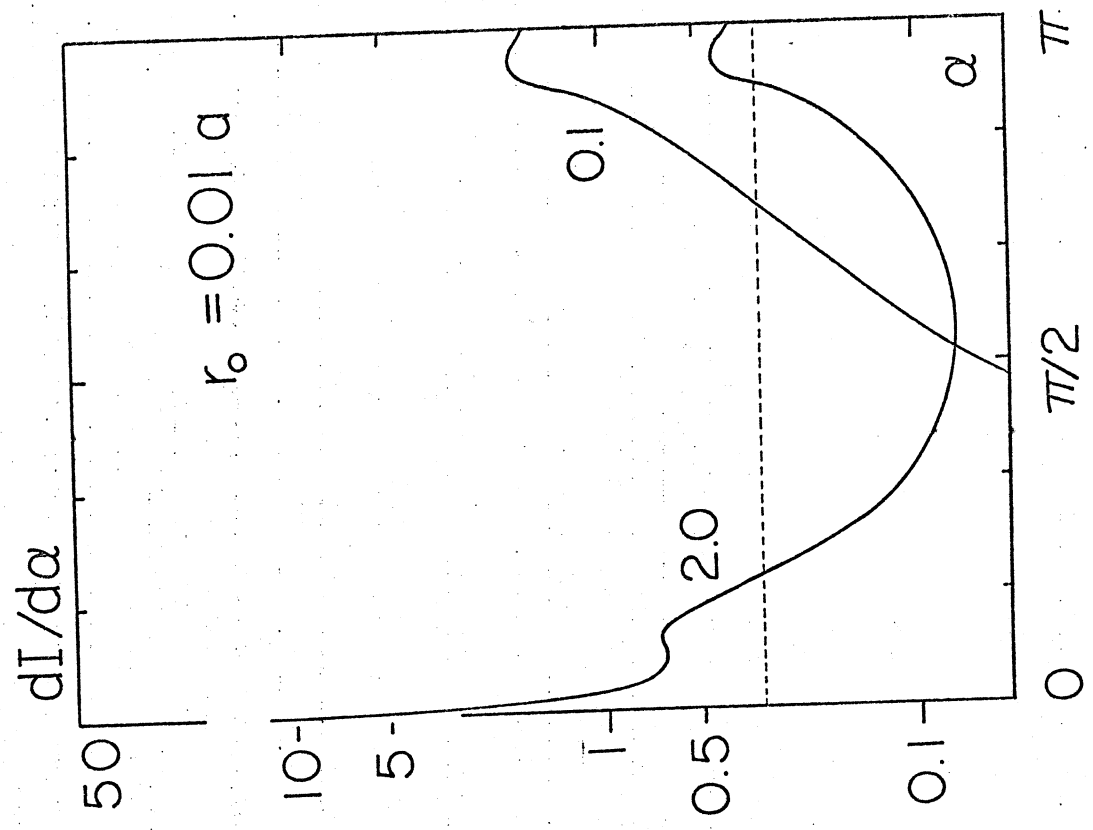
dI/dα
50
$r_o = 0.01\ a$
10
5
1
0.5
0.1
0.1
2.0
α
π
π/2
0

fig. 8

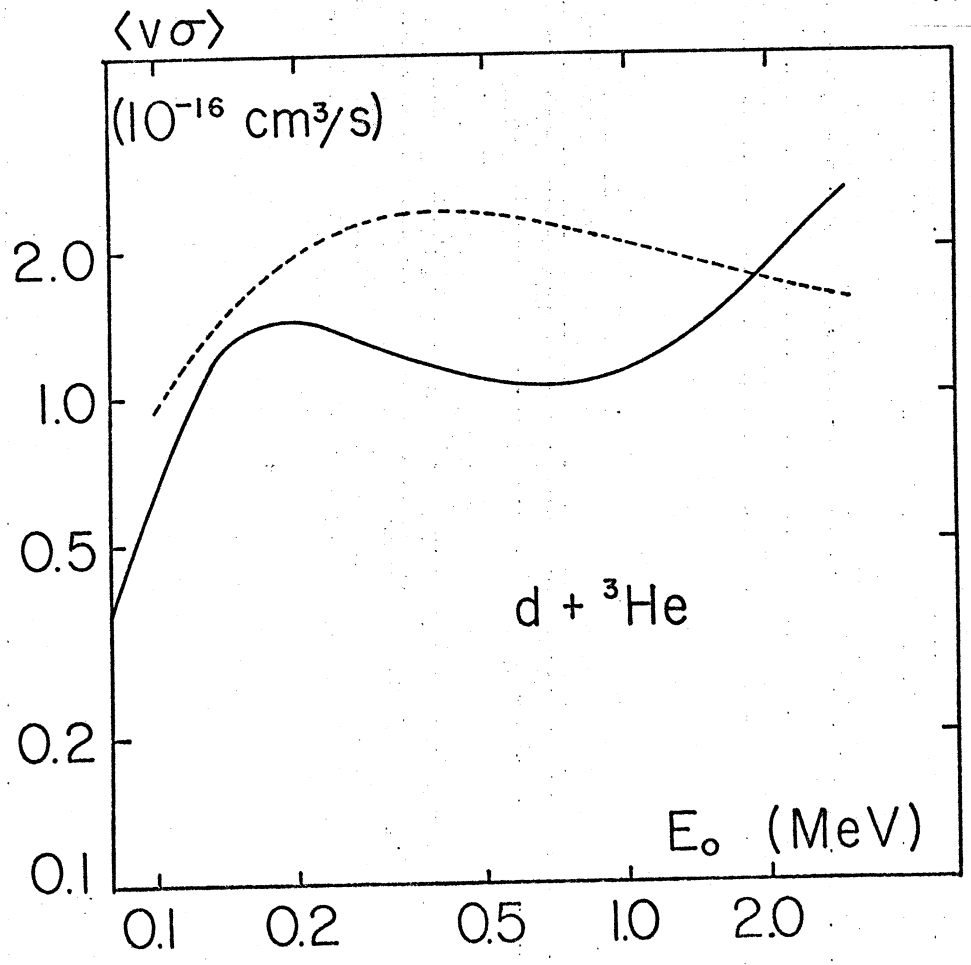
⟨vσ⟩
(10⁻¹⁶ cm³/s)
2.0
1.0
0.5
0.2
0.1
d + ³He
E₀ (MeV)
0.1
0.2
0.5
1.0
2.0